

Preparation of functional Ga₂S₃ and Ga₂Se₃ shells around Ga₂O₃ nanowires via sulfurization or selenization

Edgars Butanovs^{1,*}, Luize Dipane¹, Aleksejs Zolotarjovs¹, Sergei Vlassov², Boris Polyakov¹

¹Institute of Solid State Physics, University of Latvia, Kengaraga street 8, Riga, Latvia, LV-1063

²Institute of Physics, University of Tartu, W. Ostwaldi Str. 1, 50412, Tartu, Estonia

*e-mail: edgars.butanovs@cfi.lu.lv

Abstract

Combining defect semiconductors Ga₂S₃ and Ga₂Se₃ in Ga₂O₃-based heterostructured nanowires (NWs) have potential in photonics and optoelectronics applications due to the materials appealing optical properties. In this work, we have developed and studied Ga₂O₃-Ga₂S₃ and, for the first time, Ga₂O₃-Ga₂Se₃ *core-shell* NWs. Ga₂S₃ and Ga₂Se₃ shell was obtained during high-temperature sulfurization and selenization process of pure Ga₂O₃ NWs, respectively, in a chemical vapour transport reactor. As-grown nanostructures were characterized with scanning and transmission electron microscopy, X-ray diffraction, X-ray photoelectron spectroscopy and photoluminescence measurements. Single-nanowire photodetector devices were fabricated in order to demonstrate their electric and photoconductive properties. Such novel *core-shell* NW heterostructures could potentially be used in next-generation nanoscale electronic and optoelectronic devices.

Keywords: *nanowire; gallium oxide; Ga₂S₃; Ga₂Se₃; core-shell; heterostructure*

1. Introduction

One-dimensional (1D) nanostructures – nanowires (NWs) – have been actively investigated for different applications in nanoelectronics and optoelectronics [1], for example, photodetectors, transistors, LEDs [2–4], sensors [5,6], energy storage and

conversion [7,8] due to their unique physical characteristics, which arise from the high surface-to-volume ratio and the size confinement effects. Modification of NW surface is a promising approach how to tune their properties [9]. Compared to the conventional thin films growth, NWs surface can exhibit a considerably lessened constraint for the lattice mismatch during heterostructure preparation [10–12], therefore, making NWs as a potential template for growth of high-quality films and introducing new possibilities to engineer novel nanostructures in *core-shell* configuration [9,13].

Gallium oxide (Ga_2O_3) has recently attracted a lot of scientific attention as a prospective ultra-wide bandgap semiconductor in a form of thin films and NWs [14,15]. Ga_2O_3 has five different polymorphs among which the most stable one is monoclinic $\beta\text{-Ga}_2\text{O}_3$ with a bandgap value of around 4.9 eV [16]. While Ga_2O_3 -based thin films, NWs and heterostructures have been researched extensively in the last few years mainly for applications in power electronics [17,18] and UV photodetectors [19–21], as well as there are reports on NW sensing [22] and memory [23] devices have been demonstrated, Ga_2O_3 -based hybrid NW materials still lack the variety of studies, especially in the *core-shell* configuration. There have been only few reports over the years on $\text{Ga}_2\text{O}_3\text{-TiO}_2$ [24], $\text{Ga}_2\text{O}_3\text{-ZnO}$ [25], $\text{Ga}_2\text{O}_3\text{-WO}_3$ [26] and $\text{Ga}_2\text{O}_3\text{-Ga}_2\text{S}_3$ [27] *core-shell* NWs demonstrating the materials potential in various applications.

Gallium chalcogenide compounds can be divided in two groups based on their stoichiometry: GaX compounds, such as GaS and GaSe, are layered van der Waals materials, which have been very actively studied in the 2D form for the last decade [28–30]; and Ga_2X_3 compounds like Ga_2S_3 and Ga_2Se_3 . Ga_2S_3 and Ga_2Se_3 are commonly called ‘defect semiconductors’, since their β (monoclinic) and γ (orthorhombic) phases can be built with the cubic $\alpha\text{-Ga}_2\text{X}_3$ fundamental unit, which is basically a defect zincblende structure with the Ga/X stoichiometry ratio of only 2:3. Ordered or

randomly oriented structural Ga vacancies in the lattice result in the β - or α -phase, respectively [31–34]. Ga_2S_3 is a p-type semiconductor with a direct bandgap of 3.0-3.4 eV [31,35] and has shown promise in photonics and optoelectronics [36–38], mainly due to its intriguing optical properties, as well as in sensing [39] and possibly sodium ion batteries [40]. In comparison, Ga_2Se_3 is a slightly less studied semiconductor with the direct bandgap measured from 1.8 eV to 2.4 eV [32], which has potential applications in optoelectronic devices [31,32] and lithium ion batteries [41].

Ga_2O_3 , especially in the form of NWs, is a convenient template for Ga_2S_3 and Ga_2Se_3 growth, since synthesis of 1D Ga_2S_3 and Ga_2Se_3 nanostructures is complicated – only Ga_2Se_3 NWs growth from GaAs has been recently demonstrated [34]. It has been previously shown that Ga_2O_3 exposure to H_2S gas at elevated temperature leads to formation of either GaS or Ga_2S_3 phase [27,42] and vice versa – Ga_2O_3 was obtained via gallium sulfide annealing in an oxygen containing atmosphere [43,44]. On the other hand, to the best of our knowledge, no Ga_2O_3 - Ga_2Se_3 1D heterostructures have been previously demonstrated. Ga_2S_3 and Ga_2Se_3 are semiconductors with a narrower bandgap than Ga_2O_3 , thus giving the freedom to tune the optical properties in the visible range, especially if control over their defects could be achieved during the synthesis. Furthermore, electrical and optical properties of such heterostructures could be tuned even further through doping of the Ga_2O_3 core, either with Si or Sn to increase the electrical conductivity [16] or with rare earth elements for light emission applications [45].

In this work, we demonstrated growth of Ga_2O_3 - Ga_2S_3 and Ga_2O_3 - Ga_2Se_3 *core-shell* NWs through sulfurization and selenization, respectively, of pure Ga_2O_3 NWs at elevated temperatures. Phase composition and structural evolution was studied for samples prepared at different temperatures. Furthermore, single-nanowire

photodetector devices were fabricated in order to demonstrate their electric and photoconductive properties, which show promise for the nanostructure application in next-generation nanoscale electronic and optoelectronic devices.

2. Experimental details

Pure Ga₂O₃ NWs were grown in a horizontal quartz tube (18 mm inner diameter) reactor via atmospheric pressure chemical vapour transport (see *Fig. 1(a)*). A ceramic boat was filled with 0.15g g Ga₂O₃ powder (99.99%, *Alfa Aesar*) and loaded in the centre of the quartz tube, oxidized silicon wafers SiO₂/Si(100) (*Semiconductor Wafer, Inc.*) coated with Au nanoparticles (NPs, *Alfa Aesar*, water suspension, 100 nm diameter) were placed downstream in a lower temperature (T) region 10 cm away from the centre of the furnace. Au NPs were used as a catalyst for the vapour-liquid-solid (VLS) growth. The reactor was heated up to 1010°C (high T zone) under a flow of carrier gas mixture Ar/H₂ 5%, the temperature and flow was then maintained for 30 minutes for the NWs to grow, followed by natural cooling to the room temperature. Typically, up to 100 μm long Ga₂O₃ NWs were synthesised on the SiO₂/Si substrates, the temperature at the low T zone being around 850-900°C. Characterization data for the as-grown pure Ga₂O₃ NWs is shown in *Fig. S1*.

In order to grow either Ga₂S₃ or Ga₂Se₃ shell around Ga₂O₃ NWs, the horizontal quartz tube (18 mm inner diameter) reactor, containing Ga₂O₃ NWs in the centre (high T zone) and sulfur (99%, *Enola*) or selenium (99+%, *Alfa Aesar*) powder, respectively, upstream in the low T zone 12 cm from the centre, was heated up to the required temperature (temperatures mentioned further are in high T zone) under Ar/H₂ 5% carrier gas flow, kept for 15 minutes and then cooled naturally (see *Fig. 1(b)*). An excessive amount of sulfur and selenium powders were placed in the reactor in order to

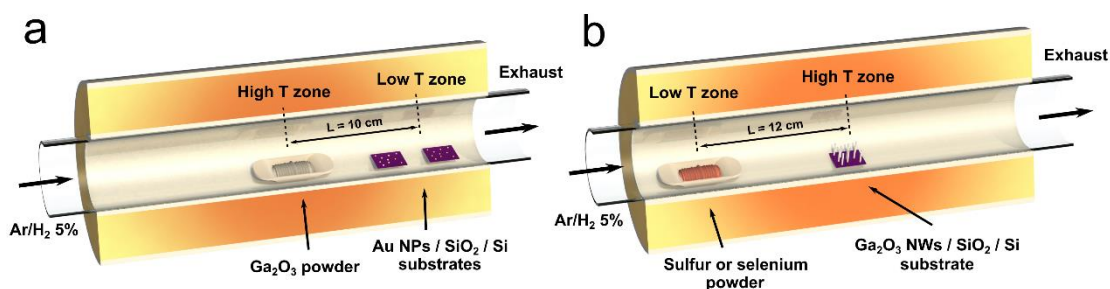


Figure 1. (a) A schematic diagram of the reactor setup used for pure Ga_2O_3 NWs growth. (b) A schematic diagram of the reactor setup used for the sulfurization and selenization of the Ga_2O_3 NWs. Sulfur and selenium powders were used as precursors for sulfurization and selenization process, respectively. The high T zone temperature corresponds to the ones used throughout the article.

maintain chalcogen-vapour-rich atmosphere. The temperature for sulfurization or selenization of Ga_2O_3 to start to occur significantly enough was found to be 400°C and 500°C , respectively. The synthesis procedures were performed at various temperatures in order to study its impact on the shell formation (growth rate, morphology, phase composition).

As-grown NW morphology was studied using a scanning electron microscope (SEM, Lyra, Tescan) together with energy dispersive X-ray (EDX) elemental analysis, while their inner crystalline structure was characterized using a transmission electron microscope (TEM, Tecnai GF20, FEI) operated at a 200 kV accelerating voltage. NW phase composition was examined by X-ray diffraction (XRD) using Rigaku MiniFlex 600 powder diffractometer with Bragg-Brentano θ - 2θ geometry and a 600W Cu anode X-ray tube (Cu $K\alpha$ line, $\lambda = 1.5406 \text{ \AA}$). Micro-Raman spectroscopy measurements were performed using a TriVista 777 confocal Raman system (Princeton Instruments, 750 mm focal length, 1800 lines/mm grating) equipped with an upright Olympus microscope with UIS2 MPlanN 100x/0.90 objective, a continuous-wave single-frequency diode-pumped laser Cobolt Samba 150 ($\lambda=532 \text{ nm}$) and Andor iDus DV420A-OE CCD camera. X-ray photoelectron spectroscopy (XPS) spectra were

obtained using an ESCALAB Xi (ThermoFisher) spectrometer. Photoluminescence (PL) spectra and its dependence on the temperature was recorded using Andor Shamrock B303-I spectrometer coupled with Andor DU401A-BV CCD camera. Sample temperature was controlled in a vacuum chamber with Sumitomo HC-4 closed-cycle helium cryostat operating within temperature range ~9–325 K. For temperature control, LakeShore 331 Temperature controller was used. Excitation of PL was performed with a 266 nm excitation wavelength - fourth harmonic of CryLas FQSS266-Q Q-switched Nd:YAG laser, with pulse energy 0.3 μJ at 15kHz. All PL spectra were not corrected to compensate for the sensitivity changes of experimental setup as only the qualitative comparison is performed.

Two-terminal individual NW photoconductor devices were fabricated via conventional photolithography process. First, NWs were mechanically transferred to an oxidized silicon wafer chip (300 nm thick SiO_2), followed by spin-coating it with AZ1518 photoresist. The optical mask with the microelectrode pattern (5 μm gap between the electrodes) was aligned on top of a single NW and exposed using SUSS MicroTec MA/BA6 Gen4 mask aligner. A 10/90/20 nm thick Cr/Ag/Al electrodes, respectively, were deposited via thermal evaporation method followed by a lift-off procedure. At least five devices for each material were fabricated in order to make consistent conclusions. Current–voltage (I – V) characteristics and photoresponse of the fabricated single-NW photodetector devices were measured with a two-contact microprobe station connected to a low-noise current preamplifier (SR570, Stanford Research Systems) and oscilloscope (TDS2004B, Tektronix). A 405 nm wavelength semiconductor diode laser (CNI Laser) with 0.5 W/cm^2 power was the illumination source for the photoresponse measurements. All the measurements were performed at room temperature and in air.

3. Results and discussion

As-grown *core-shell* NW morphology and the inner structure was characterized using TEM (see Fig. 2). In the case of sulfurized Ga_2O_3 NWs, it was possible to obtain a continuous, few nanometres thick Ga_2S_3 shell around NWs at 600°C (Fig. 2(a)). A uniform shell is a prerequisite for good electrical properties of the nanostructure. On the other hand, protruding GaS crystals start to form at such temperature as has been shown at a higher resolution in Fig. 2(c). Similarly, a continuous Ga_2Se_3 shell was obtained after selenization of Ga_2O_3 NWs at 600°C (see Fig. 2 (e)). Here, the shell is smoother in comparison to the sulfurized NWs, since only one new phase forms. The NWs maintain their length after sulfurization/selenization and the formed shell is

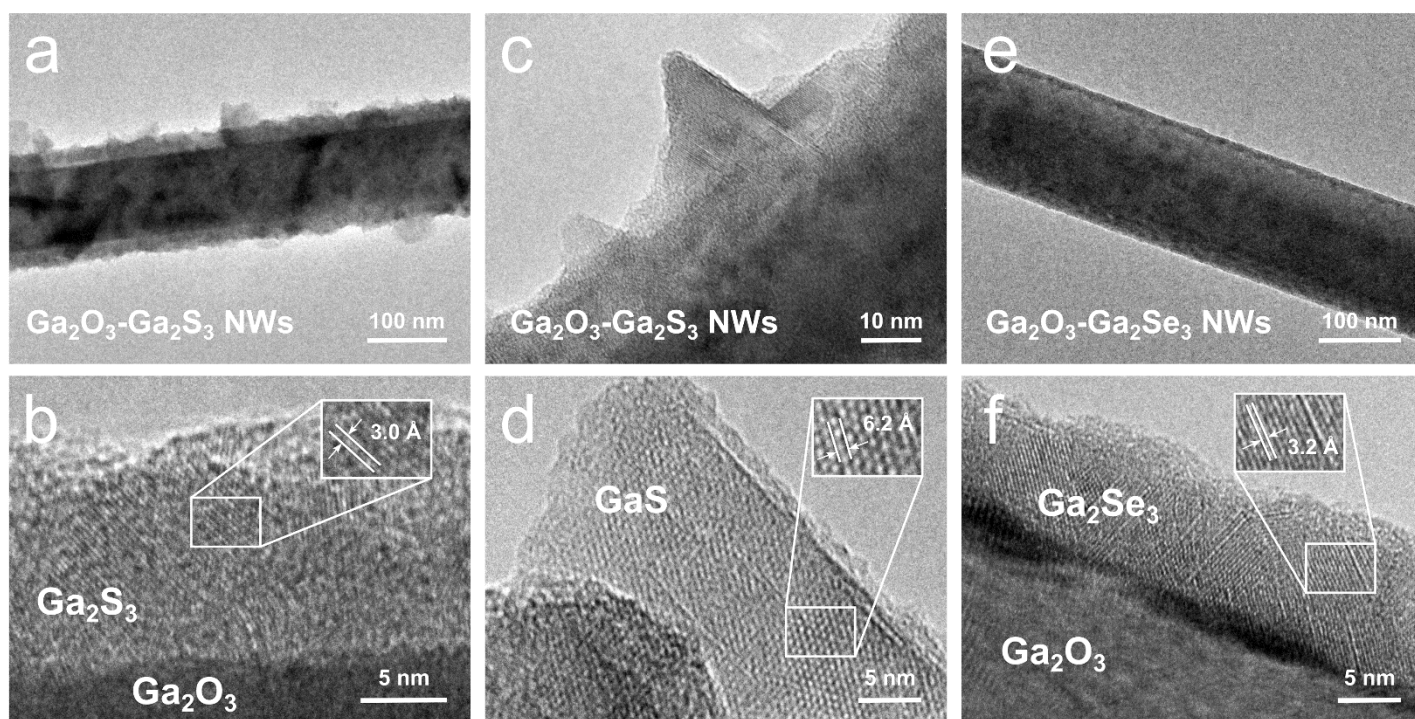


Figure 2. Transmission electron microscope images at different magnifications of (a-d) Ga_2O_3 - Ga_2S_3 *core-shell* NWs prepared at 600°C and (e,f) Ga_2O_3 - Ga_2Se_3 *core-shell* NWs prepared at 500°C . Note that Ga_2O_3 NWs sulfurized at higher temperatures also contain crystals of GaS phase. The insets show the measured atomic interlayer distances in the formed phases.

uniformly distributed along the NWs, as was confirmed by SEM and EDX measurements (see *Fig. S2*), however, the surface roughness of the *core-shell* NWs increases at higher temperatures (see *Fig. S3*) because of the more active reaction between Ga₂O₃ and the chalcogenide vapour. In order to control the shell thickness, process time can be used with some limitations. At higher TEM resolution (*Fig. 2(b,d,f)*) the inner crystalline structure of the formed phases is revealed and interplanar distance values measured. Interplanar distance in the Ga₂S₃ shell was determined to be 3.0 Å, which is in a good agreement with the lattice parameter $c=6.031\text{Å}$ in ICDD-PDF #48-1434. The protruding GaS crystals exhibit interplanar distance of 6.2 Å, which corresponds to lattice spacing between (101) planes in GaS [46]. As for the Ga₂Se₃ shell, interplanar distance was measured to be 3.2-3.3Å, closely matching the lattice parameter $c=6.6491\text{Å}$ in ICDD-PDF #44-1012. The TEM measurements show the high crystalline quality of the prepared *core-shell* NWs. The processed NWs preserve their length, inner composition and crystalline structure in comparison to pure Ga₂O₃ NWs, since the reaction with chalcogenide vapour occurs close to the surface, mainly leading to morphological changes.

To confirm the presence of the phases in the as-grown *core-shell* NW samples, XRD measurements were performed on the NW arrays on the Si(100)/SiO₂ substrates, prepared at various temperatures (see *Fig. 3*). Worth noting that all the unmarked peaks belong to the monoclinic Ga₂O₃ core (ICDD-PDF #41-1103) and are interpreted in *Fig. S1(a)*. In the case of the sulfurized Ga₂O₃ NWs (*Fig. 2(a)*), formation of monoclinic Ga₂S₃ phase (ICDD-PDF #48-1434) takes place in the whole tested temperature range from 400°C to 600°C. On the other hand, hexagonal GaS phase (ICDD-PDF #48-1435) start to appear at 520°C and above. As for the selenized Ga₂O₃ NWs (*Fig. 3(b)*), monoclinic Ga₂Se₃ phase (ICDD-PDF #44-1012) is present in the samples prepared at

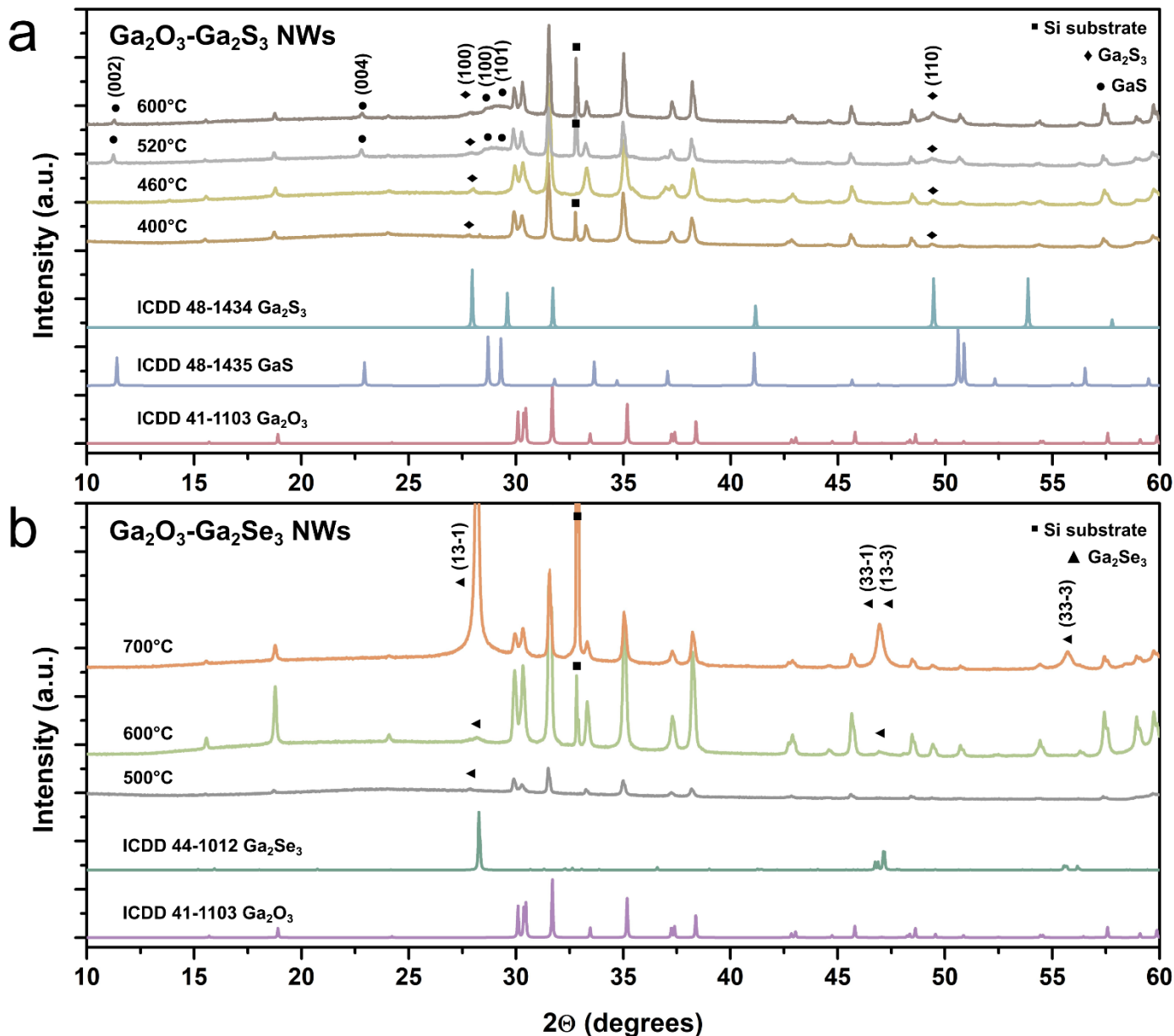


Figure 3. X-ray diffraction patterns of (a) $\text{Ga}_2\text{O}_3\text{-Ga}_2\text{S}_3$ and (b) $\text{Ga}_2\text{O}_3\text{-Ga}_2\text{Se}_3$ core-shell NW arrays on Si(100)/ SiO_2 substrates, prepared at various temperatures. The respective ICDD patterns for each phase are provided for reference.

temperatures starting from 500°C and above. The intensity of the Ga_2Se_2 peaks in relation to the Ga_2O_3 ones increases significantly with rising temperature, indicating that selenium vapour reacts more aggressively with Ga_2O_3 NWs. This is accompanied by significant increase of surface roughness, as can be seen in *Fig.S3*. Bragg peak at $2\theta \approx 33^\circ$ can be attributed to the Si(100) substrate (forbidden Si(200) reflection). XRD results match well with the visual observations made by TEM – the samples with the

visible protruding crystals correspond to the ones containing GaS phase. The formation of the hexagonal phase during the sulfurization and not during selenization could occur because sulfur and H₂S vapour are not as reactive as the selenium counterparts, which might lead to anion deficiency and preferable formation of GaS phase alongside Ga₂S₃ in our tested synthesis parameter range. On the other hand, the chemically more active selenium and H₂Se vapour leads to the cation deficient Ga₂Se₃ phase [47]. GaSe can be produced from Ga₂Se₃ at higher temperatures (960°C) and lower pressure (330 Pa) as it was shown by Wu *et al.* [48]. In our case the synthesis was carried out at atmospheric pressure in a temperature range 500-700°C resulting in pure Ga₂Se₃ shell formation. Furthermore, since GaS hexagonal layered crystal structure does not match the Ga₂S₃ monoclinic structure, GaS crystals grow outwards due to the large lattice mismatch.

Room-temperature micro-Raman spectroscopy was used to confirm the presence of the respective compounds in the as-prepared *core-shell* NWs. Raman

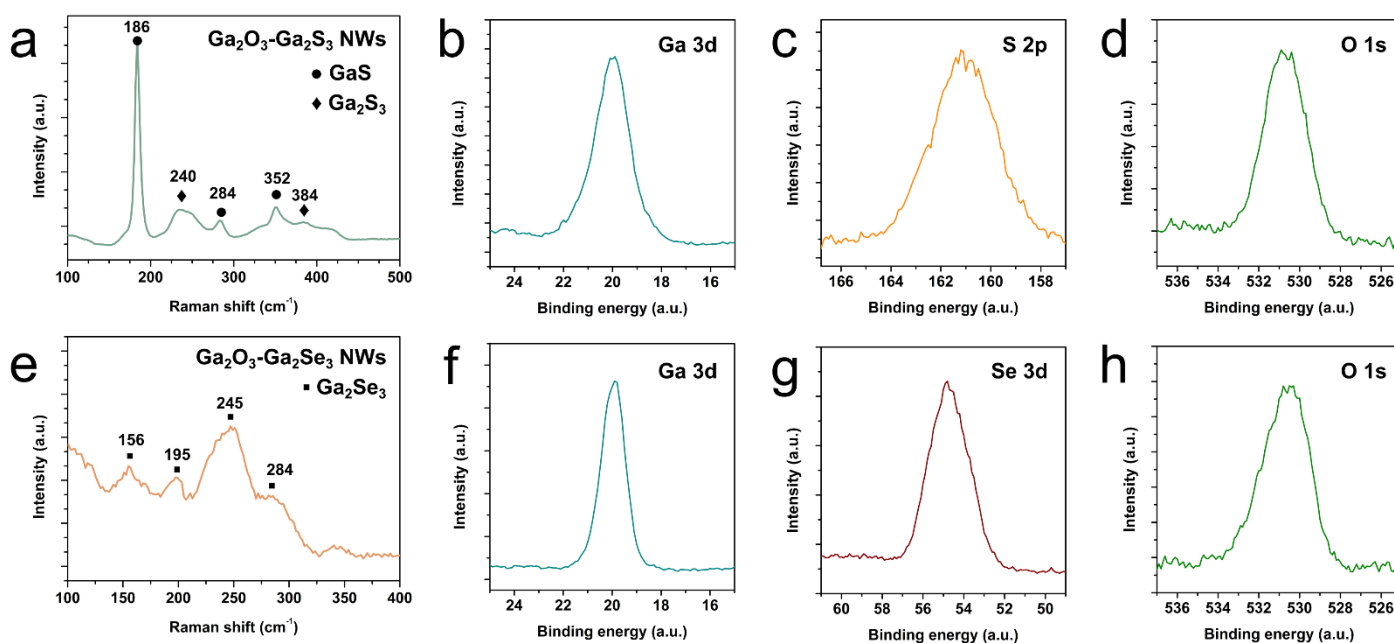


Figure 4. Micro-Raman spectra of (a) Ga₂O₃-Ga₂S₃ and (e) Ga₂O₃-Ga₂Se₃ *core-shell* NWs, both prepared at 600°C. XPS spectra of the same (b-d) Ga₂O₃-Ga₂S₃ and (f-h) Ga₂O₃-Ga₂Se₃ NWs, showing the peak scans of the detected elements.

spectra of Ga₂O₃-Ga₂S₃ NWs (*Fig. 4(a)*) contains several peaks: the ones at 186, 284 and 352 cm⁻¹ can be attributed to GaS A_{1g}, E_{2g}¹ and A_{2g}¹ modes, respectively [49], while the 240 and a weaker 384 cm⁻¹ peak belong to Ga₂S₃ A_{1g} and F_{2g} modes, respectively [37]. As for Ga₂O₃-Ga₂Se₃ *core-shell* NWs (see *Fig. 4(e)*), Raman peak features measured at 156, 195, 245 and 284 cm⁻¹ can be indexed to A₁, A₁, A' and F₂ vibration modes in Ga₂Se₃, respectively [32]. Furthermore, an XPS analysis was performed in order to verify the chemical composition of the *core-shell* NW arrays on the Si(100)/SiO₂ substrates. Survey spectra are depicted in *Fig. S4(a,b)* and did not contain any peaks of possible contaminant elements. High-resolution spectra of Ga3d, O1s, S2p and Se3d were acquired (see *Fig. 4(b-d)* and *(f-h)* for sulfurized and selenized Ga₂O₃ NWs, respectively) and calibrated relative to adventitious C 1s peak at 285 eV binding energy. None of the peaks exhibited any observable shift in binding energy due to the change of the chemical states after sulfurization or selenization, as well as no distinction between Ga₂S₃ and GaS chemical states was possible to be made. The characteristic Ga3d peak is located at 20.2 eV binding energy, while the O1s peak at around 530.4 eV. After sulfurization of Ga₂O₃ NWs, S2p peak, characteristic for metal sulfides, emerged at 161.3 eV. Worth noting that S2p peak in gallium sulfide compounds also contains contribution of Ga2s peak, as shown in the fitted scan in *Fig. S4(c)*. Lastly, Ga₂O₃-Ga₂Se₃ *core-shell* NW samples exhibited Se3d peak at 54.8 eV, thus confirming the formation of a selenide compound in the nanostructures.

PL spectra, measured at room and 30K temperature, for Ga₂O₃-Ga₂S₃ and Ga₂O₃-Ga₂Se₃ *core-shell* NWs and pure Ga₂O₃ NWs are depicted in Fig. 5. The PL intensity is depicted in arbitrary units and does not contain information about relative intensities between the measured spectra. PL of all samples consists of many overlapping peaks and thus analysis is challenging; however, some features can be identified. Pure Ga₂O₃ (see Fig.5(a)) commonly exhibits a wide blue-green PL defect band ranging from around 380 to 650 nm, which is well studied and consists of various overlapping contributions of recombination between donor and acceptor bands, formed by oxygen vacancy / Ga²⁺ and gallium vacancy / gallium-oxygen vacancy pairs, respectively [50,51]. This blue-green Ga₂O₃ defect band is present in all the measured spectra for the sulfurized and selenized samples. The PL spectrum of the Ga₂O₃-Ga₂S₃ NWs (see Fig.5(b)) contains another defect band centred at around 680 nm, which is attributed to transition between two deep acceptor and donor levels in Ga₂S₃, located at 0.4 eV above the valence band and 1.1 eV below the conduction band, respectively [27,35]. Some contribution to the PL spectrum might also come from GaS [52]. As for the Ga₂O₃-Ga₂Se₃ *core-shell* NW PL spectrum (see Fig.5(c)), two peaks can be resolved at 645 and 695 nm while measuring at 30K, matching free exciton and bound

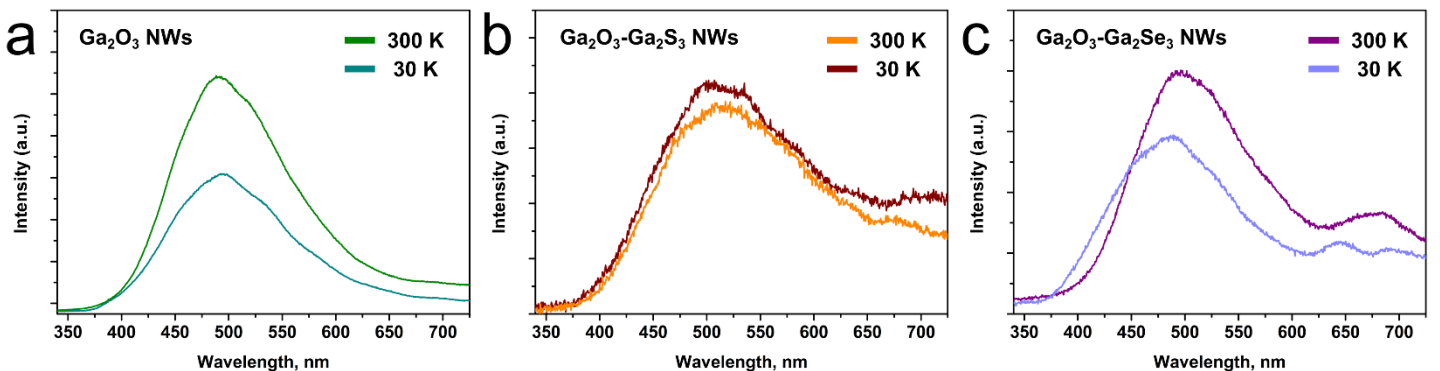


Figure 5. Photoluminescence spectra of (a) pure Ga₂O₃, (b) sulfurized and (c) selenized (both at 600°C) NW array. Spectra were measured at 30K and room temperature with 266 nm excitation wavelength.

exciton emissions in Ga₂Se₃, respectively [32]. At room measurement temperature only one peak can be distinguished at 680 nm, which consists of contributions from the band-edge free exciton combined with the bound exciton and defect emissions, as previously shown by Ho [32].

Two-terminal single-nanowire photodetectors were fabricated from the as-prepared *core-shell* NWs, as well as from the pure Ga₂O₃ NWs. Ga₂O₃ NWs exhibited very low conductivity (see *Fig.S5*) and no response to visible light. *Fig. 6(a)* and *(c)* shows the measured dark state current-voltage (I-V) characteristics for Ga₂O₃-Ga₂S₃ (prepared at 600°C) and Ga₂O₃-Ga₂Se₃ (prepared at 500°C) *core-shell* NWs, respectively. The insets show optical microscope images of typical single-nanowire two-terminal photodetector devices for each material. I-V curve for Ga₂O₃-Ga₂S₃ NWs shows linear behaviour, indicating that ohmic contacts formed between Cr layers in electrodes and Ga₂S₃ as has been demonstrated previously [39]. In contrast, the I-V curve for Ga₂O₃-Ga₂Se₃ NWs exhibits asymmetric Schottky behaviour in pA range [33]. The strong current saturation at higher positive bias voltages could be explained by contribution of space-charge limited current (SCLC), which is often observed in nanoscale devices when charge carriers are forced into small volume and start screening each other [53]. Since the pure Ga₂O₃ NWs demonstrated very poor conductivity, most probably the current in the prepared *core-shell* NWs mainly flows through the few nanometres thick shell. The devices were periodically illuminated with 405 nm wavelength light in order to study their photoresponse properties as shown in *Fig. 6(b)* and *(d)* for Ga₂O₃-Ga₂S₃ and Ga₂O₃-Ga₂Se₃ *core-shell* NWs, respectively. The devices were also tested for 532 nm and 660 nm laser light; however, no response was observed. On-off measurements demonstrate a steady, rapid and repeatable increase and decrease of the current when the illumination of Ga₂O₃-Ga₂S₃ NWs is turned on or off,

respectively; therefore, showing good stability and reversibility of the devices. Rise and decay time of the devices, defined as the required time for the photocurrent to increase or decrease to 90% or 10%, was determined to be around 30 ms. Important to note that the role of the GaS phase, present in the $\text{Ga}_2\text{O}_3\text{-Ga}_2\text{S}_3$ *core-shell* NWs, on device performance is still unclear and should be elucidated – presumably the mixture of two semiconductors introduces structural defects, which degrade the electrical properties of the shell. Similar results were obtained for $\text{Ga}_2\text{O}_3\text{-Ga}_2\text{Se}_3$ *core-shell* NW devices, however, the dark current (around 1 nA) and the generated photocurrent (3-4 nA) was more than a magnitude higher (tens of pA in Ga_2S_3), meaning higher responsivity, and the rise and decay time was measured to be around 40 and 900 ms, respectively. The longer decay time is typically associated with charge carrier trapping centres [54]. The current enhancement ratios ($I_{\text{on}}/I_{\text{off}}$) for the both prepared materials nanostructures were

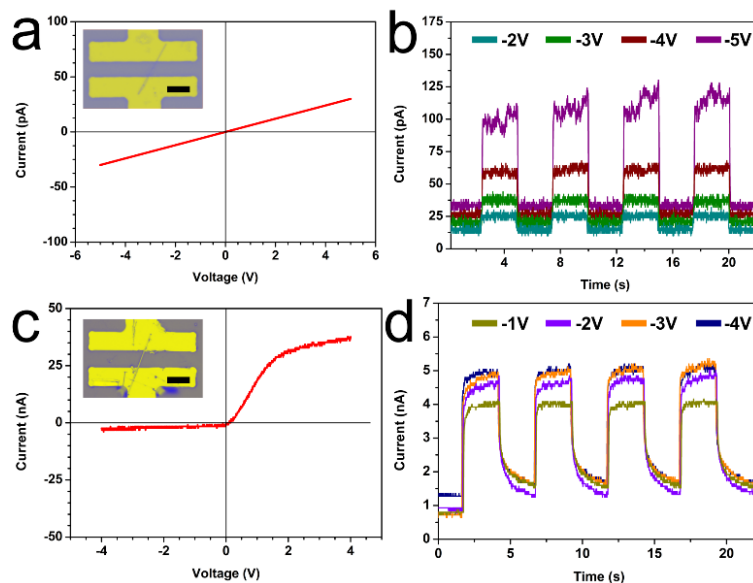


Figure 6. $\text{Ga}_2\text{O}_3\text{-Ga}_2\text{S}_3$ single nanowire, prepared at 600°C , (a) dark state I-V characteristics, (b) on-off photoresponse at different bias voltages. $\text{Ga}_2\text{O}_3\text{-Ga}_2\text{Se}_3$ single nanowire, prepared at 500°C , (c) dark state I-V characteristics, (d) on-off photoresponse at different bias voltages. 405 nm wavelength light with 0.5 W/cm^2 intensity was used for illumination in the photoresponse measurements. The insets show optical microscope images of typical single-nanowire two-terminal photodetector devices for each material. Scale bars correspond to $10 \mu\text{m}$.

measured to be at around 4-5. Ultimately, Ga₂O₃ NWs show promise as a convenient template for Ga₂S₃ and Ga₂Se₃ semiconductor growth, which could enable the materials applicability in next-generation nanoscale optoelectronic devices, such as photodetectors.

5. Conclusions

In this work, we demonstrated growth of Ga₂O₃-Ga₂S₃ and Ga₂O₃-Ga₂Se₃ *core-shell* NWs, in which the shell was obtained during high-temperature sulfurization and selenization process of pure Ga₂O₃ NWs, respectively, in a chemical vapour transport reactor. Synthesis of pure Ga₂S₃ and Ga₂Se₃ 1D nanostructures is complicated, however, Ga₂O₃ is a convenient template for Ga₂S₃ and Ga₂Se₃ growth due to the simple synthesis process and the similar crystal structures. In the case of sulfurization, Ga₂S₃ shell formation was observed above 400°C, however, GaS phase also forms as protruding crystallites at temperatures higher than 520°C. As for Ga₂Se₃, formation of other phases was not observed at 500-700°C. Generally, at lower reaction temperatures continuous, few nanometres thick shells grow, while higher process temperature leads to increase of nanostructure surface roughness. Furthermore, single-nanowire photodetector devices were fabricated in order to demonstrate their electric and photoconductive properties, which show promise for the nanostructure application in next-generation nanoscale electronic and optoelectronic devices.

Acknowledgements

This research is funded by the Latvian Council of Science project “Epitaxial Ga₂O₃ thin films as ultrawide bandgap topological transparent electrodes for ultraviolet optoelectronics” No. lzp-2020/1-0345. S.V. was supported by the European

Union's Horizon 2020 program, under Grant Agreement No. 856705 (ERA Chair “MATTER”). Institute of Solid State Physics, University of Latvia as the Center of Excellence has received funding from the European Union’s Horizon 2020 Framework Programme H2020-WIDESPREAD-01-2016-2017-TeamingPhase2 under grant agreement No. 739508, project CAMART². The authors are grateful to Jevgenijs Gabrusenoks for micro-Raman measurements and Valts Minders for assistance with materials synthesis.

Supplementary information

Supplementary information is available and contains characterization data on pure Ga₂O₃ NWs, SEM images of the *core-shell* NWs prepared at different temperatures, XPS survey spectra and detailed analysis of S2p peak, and dark-state I-V curve of single Ga₂O₃ nanowire two-terminal device.

References

- [1] Dasgupta, N. P. *et al.* 25th Anniversary Article: Semiconductor Nanowires - Synthesis, Characterization, and Applications. *Adv. Mater.* **26**, 2137–2184 (2014)
- [2] Jia, C., Lin, Z., Huang, Y. & Duan, X. Nanowire Electronics: From Nanoscale to Macroscale. *Chem. Rev.* **119**, 9074–9135 (2019)
- [3] Soci, C. *et al.* Nanowire Photodetectors. *J. Nanosci. Nanotechnol.* **10**, 1430–1449 (2010)
- [4] Yan, R., Gargas, D. & Yang, P. Nanowire photonics. *Nat. Photonics* **3**, 569–576 (2009)
- [5] Fennell, J. F. *et al.* Nanowire Chemical/Biological Sensors: Status and a Roadmap for the Future. *Angew. Chemie Int. Ed.* **55**, 1266–1281 (2016)

- [6] Chen, X., Wong, C. K. Y., Yuan, C. A. & Zhang, G. Nanowire-based gas sensors. *Sensors Actuators B Chem.* **177**, 178–195 (2013)
- [7] Mai, L., Tian, X., Xu, X., Chang, L. & Xu, L. Nanowire Electrodes for Electrochemical Energy Storage Devices. *Chem. Rev.* **114**, 11828–11862 (2014)
- [8] Chen, Z. *et al.* Core–shell MoO₃–MoS₂ Nanowires for Hydrogen Evolution: A Functional Design for Electrocatalytic Materials. *Nano Lett.* **11**, 4168–4175 (2011)
- [9] Sun, Y., Sun, B., He, J. & Wang, C. Compositional and structural engineering of inorganic nanowires toward advanced properties and applications. *InfoMat* **1**, 496–524 (2019)
- [10] Li, Y., Qian, F., Xiang, J. & Lieber, C. M. Nanowire electronic and optoelectronic devices. *Mater. Today* **9**, 18–27 (2006)
- [11] Dong, Y., Tian, B., Kempa, T. J. & Lieber, C. M. Coaxial Group III–Nitride Nanowire Photovoltaics. *Nano Lett.* **9**, 2183–2187 (2009)
- [12] Polyakov, B. *et al.* Unexpected Epitaxial Growth of a Few WS₂ Layers on {1100} Facets of ZnO Nanowires. *J. Phys. Chem. C* **120**, 21451–21459 (2016)
- [13] Butanovs, E. *et al.* Synthesis and characterization of GaN/ReS₂, ZnS/ReS₂ and ZnO/ReS₂ core/shell nanowire heterostructures. *Appl. Surf. Sci.* **536**, 147841 (2021)
- [14] Yuan, Y. *et al.* Toward emerging gallium oxide semiconductors: A roadmap. *Fundam. Res.* **1**, 697–716 (2021)
- [15] Pearton, S. J. *et al.* A review of Ga₂O₃ materials, processing, and devices. *Appl. Phys. Rev.* **5**, 011301 (2018)
- [16] Teherani, F. H. *et al.* A review of the growth, doping, and applications of β-

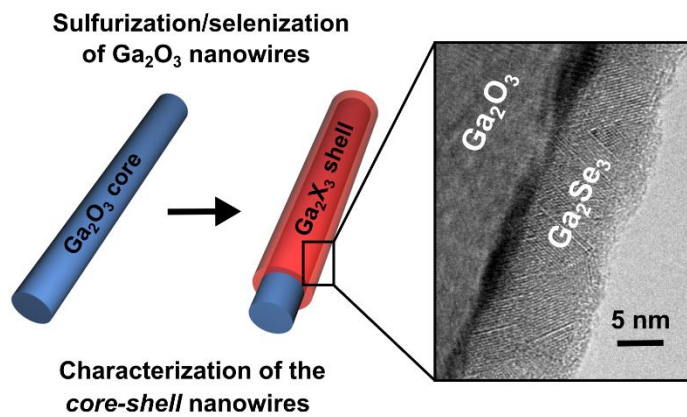
- Ga₂O₃ thin films. *Proc. SPIE 10533, Oxide-based Mater. Devices IX, 105330R* (2018)
- [17] Pearton, S. J., Ren, F., Tadjer, M. & Kim, J. Perspective: Ga₂O₃ for ultra-high power rectifiers and MOSFETS. *J. Appl. Phys.* **124**, 220901 (2018)
- [18] Perez-Tomas, A., Chikoidze, E. & Rogers, D. J. A walk on the frontier of energy electronics with power ultra-wide bandgap oxides and ultra-thin neuromorphic 2D materials. in *Oxide-based Materials and Devices XII* (eds. Teherani, F. H., Look, D. C. & Rogers, D. J.) 63 (SPIE, 2021)
doi:10.1117/12.2590747
- [19] Kaur, D. & Kumar, M. A Strategic Review on Gallium Oxide Based Deep-Ultraviolet Photodetectors: Recent Progress and Future Prospects. *Adv. Opt. Mater.* **9**, 2002160 (2021)
- [20] Xie, C. *et al.* Catalyst-Free Vapor–Solid Deposition Growth of β -Ga₂O₃ Nanowires for DUV Photodetector and Image Sensor Application. *Adv. Opt. Mater.* **7**, 1901257 (2019)
- [21] Wang, S. *et al.* In situ synthesis of monoclinic β -Ga₂O₃ nanowires on flexible substrate and solar-blind photodetector. *J. Alloys Compd.* **787**, 133–139 (2019)
- [22] Afzal, A. β -Ga₂O₃ nanowires and thin films for metal oxide semiconductor gas sensors: Sensing mechanisms and performance enhancement strategies. *J. Mater.* **5**, 542–557 (2019)
- [23] Sivakumar, C. *et al.* High-Quality Single-Crystalline β -Ga₂O₃ Nanowires: Synthesis to Nonvolatile Memory Applications. *Nanomaterials* **11**, 2013 (2021)
- [24] Chang, K.-W. & Wu, J.-J. Formation of β -Ga₂O₃-TiO₂ Nanobarcodes from Core-Shell Nanowires. *Adv. Mater.* **17**, 241–245 (2005)

- [25] Jin, C., Park, S., Kim, H. & Lee, C. Ultrasensitive multiple networked Ga₂O₃-core/ZnO-shell nanorod gas sensors. *Sensors Actuators B Chem.* **161**, 223–228 (2012)
- [26] Park, S., Kim, S., Sun, G. J. & Lee, C. Synthesis, structure and ethanol sensing properties of Ga₂O₃-core/WO₃-shell nanostructures. *Thin Solid Films* **591**, 341–345 (2015)
- [27] Othonos, K. M., Zervos, M., Christofides, C. & Othonos, A. Ultrafast Spectroscopy and Red Emission from β -Ga₂O₃/ β -Ga₂S₃ Nanowires. *Nanoscale Res. Lett.* **10**, 304 (2015)
- [28] Late, D. J. *et al.* GaS and GaSe Ultrathin Layer Transistors. *Adv. Mater.* **24**, 3549–3554 (2012)
- [29] Hu, P. *et al.* Highly Responsive Ultrathin GaS Nanosheet Photodetectors on Rigid and Flexible Substrates. *Nano Lett.* **13**, 1649–1654 (2013)
- [30] Jung, C. S. *et al.* Red-to-Ultraviolet Emission Tuning of Two-Dimensional Gallium Sulfide/Selenide. *ACS Nano* **9**, 9585–9593 (2015)
- [31] Ho, C.-H., Lai, X.-R., Chuang, C.-A., Kuo, W.-L. & Tiong, K.-K. The Study of Optical Properties of III₂–VI₃ Defect Semiconductor Group Compounds Ga₂S₃, Ga₂Se₃, In₂S₃, and In₂Se₃. *Adv. Photonics Res.* **2**, 2000110 (2021)
- [32] Ho, C.-H. Ga₂Se₃ Defect Semiconductors: The Study of Direct Band Edge and Optical Properties. *ACS Omega* **5**, 18527–18534 (2020)
- [33] Xue, W. *et al.* Discovery of Robust Ferroelectricity in 2D Defective Semiconductor α -Ga₂Se₃. *Small* **18**, 2105599 (2022)
- [34] Berto, F. *et al.* Ga₂Se₃ Nanowires via Au-Assisted Heterovalent Exchange Reaction on GaAs. *J. Phys. Chem. C* **124**, 17783–17794 (2020)
- [35] Yoon, C.-S. *et al.* Blue photoluminescence of α -Ga₂S₃ and α -Ga₂S₃:Fe²⁺

- single crystals. *Appl. Phys. Lett.* **83**, 1947–1949 (2003)
- [36] Liu, H. F. *et al.* Synthesis and Phase Evolutions in Layered Structure of Ga₂S₃ Semiconductor Thin Films on Epiready GaAs (111) Substrates. *ACS Appl. Mater. Interfaces* **6**, 3501–3507 (2014)
- [37] Zheng, Y., Tang, X., Wang, W., Jin, L. & Li, G. Large-Size Ultrathin α -Ga₂S₃ Nanosheets Toward High-Performance Photodetection. *Adv. Funct. Mater.* **31**, 2008307 (2021)
- [38] Ho, C.-H. & Chen, H.-H. Optically decomposed near-band-edge structure and excitonic transitions in Ga₂S₃. *Sci. Rep.* **4**, 6143 (2015)
- [39] Alsaif, M. M. Y. A. *et al.* Atomically Thin Ga₂S₃ from Skin of Liquid Metals for Electrical, Optical, and Sensing Applications. *ACS Appl. Nano Mater.* **2**, 4665–4672 (2019)
- [40] Wang, P. *et al.* Exploring the sodium ion storage mechanism of gallium sulfide (Ga₂S₃): a combined experimental and theoretical approach. *Nanoscale* **11**, 3208–3215 (2019)
- [41] Ding, J.-J., Zhou, Y.-N., Cui, Y.-H. & Fu, Z.-W. Ga₂Se₃ Thin Film as a Negative Electrode Material for Lithium-Ion Batteries. *ECS Electrochem. Lett.* **1**, A7–A9 (2012)
- [42] Zervos, M., Othonos, A., Gianneta, V., Travlos, A. & Nassiopoulou, A. G. Sn doped β -Ga₂O₃ and β -Ga₂S₃ nanowires with red emission for solar energy spectral shifting. *J. Appl. Phys.* **118**, (2015)
- [43] Leontie, L. *et al.* Synthesis and optical properties of Ga₂O₃ nanowires grown on GaS substrate. *Thin Solid Films* **689**, (2019)
- [44] Sprincean, V. *et al.* Crystallinity and optical properties of β -Ga₂O₃/Ga₂S₃ layered structure obtained by thermal annealing of Ga₂S₃ semiconductor.

- Mater. Sci. Semicond. Process.* **121**, 105314 (2021)
- [45] Khartsev, S. *et al.* Reverse-Bias Electroluminescence in Er-Doped β -Ga₂O₃ Schottky Barrier Diodes Manufactured by Pulsed Laser Deposition. *Phys. Status Solidi Appl. Mater. Sci.* **219**, 1–5 (2022)
- [46] Carey, B. J. *et al.* Wafer-scale two-dimensional semiconductors from printed oxide skin of liquid metals. *Nat. Commun.* **8**, 14482 (2017)
- [47] Liu, J. *et al.* Self-assembled epitaxy of Ga₂Se₃ on the oxidized GaSe surface and atomic imaging of the Ga₂Se₃/GaSe heterostructure. *Appl. Surf. Sci.* **586**, 152774 (2022)
- [48] Wu, C.-Y. *et al.* Controlled synthesis of GaSe microbelts for high-gain photodetectors induced by the electron trapping effect. *J. Mater. Chem. C* **8**, 5375–5379 (2020)
- [49] Yang, S. *et al.* High performance few-layer GaS photodetector and its unique photo-response in different gas environments. *Nanoscale* **6**, 2582–2587 (2014)
- [50] Mi, W. *et al.* Ultraviolet–green photoluminescence of β -Ga₂O₃ films deposited on MgAl₆O₁₀ (100) substrate. *Opt. Mater. (Amst)*. **35**, 2624–2628 (2013)
- [51] Yu, D. ., Bubendorff, J.-L., Zhou, J. ., Leprince-Wang, Y. & Troyon, M. Localized cathodoluminescence investigation on single Ga₂O₃ nanoribbon/nanowire. *Solid State Commun.* **124**, 417–421 (2002)
- [52] Chiricenco, V., Caraman, M., Rusu, I. . & Leontie, L. On the luminescence of GaS(Cu) single crystals. *J. Lumin.* **101**, 71–77 (2003)
- [53] Zhang, P. *et al.* Space–charge limited current in nanodiodes: Ballistic, collisional, and dynamical effects. *J. Appl. Phys.* **129**, 100902 (2021)
- [54] Jiang, J. *et al.* Defect Engineering for Modulating the Trap States in 2D Photoconductors. *Adv. Mater.* **30**, 1804332 (2018)

Graphical abstract



Single-nanowire device
photoresponse to 405nm light

